Excursions of a complex analyst
into the realm of dynamical systems

Eric Bedford

§0. Introduction

The purpose of this talk is to discuss some connections between dynamics and complex analysis, especially the aspects of dynamical systems that were sufficiently interesting to me to make me drop what I was doing several years ago and enter into a long collaboration with John Smillie. One of the motivations for the work with Smillie has been to consider the dynamics of a polynomial diffeomorphism f of $\mathbf{C}^2$ which is the complexification of a map of $\mathbf{R}^2$. In general, the dynamical systems induced by f on $\mathbf{R}^2$ and $\mathbf{C}^2$ can be considerably different. However, if the complex Julia set $J \subset \mathbf{C}^2$ also happens to be a subset of $\mathbf{R}^2$, then in addition to the usual tools of real dynamics, we may also use complex methods. In the following talk, we will present the approach developed with Smillie in [BS1–5]. In §3, we outline the work [BD1,2] with Jeff Diller in which this same approach has been applied to a family of birational maps of the plane. In §4 we describe the Hénon attractor in $\mathbf{R}^2$, for which it has been difficult to actually prove anything. Although it is speculative, we present the suggestion that this phenomenon might profitably be investigated in the complex domain, a suggestion that I think Oka might have found intriguing. Given the constraints of space and time, I have limited myself to expounding a point of view and have made no attempt to survey the literature.[1]

[1]We recommend [MNTU] for an extended introduction to the dynamics of polynomial diffeomorphisms of $\mathbf{C}^2$ and Sibony [S] for a unified treatment of the iteration of rational mappings of $\mathbf{P}^k$.
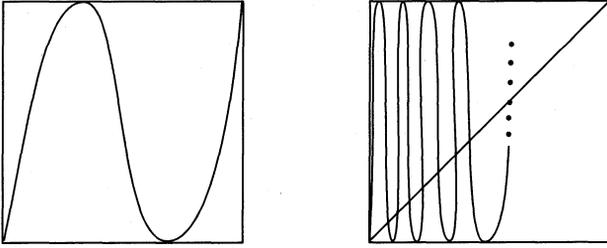
E. Bedford

Figure 1. Graph of Γ_f (on left) and Γ_{f^n} intersected with the diagonal

In the study of dynamical systems, we consider a self mapping $f :$ $X \to X$ of a space X and describe the behavior of its iterates $f^n = f \circ \cdots \circ f$ as $n \to \infty$. It is not clear at the outset exactly which connections this might have with the questions and techniques of analysis. If $f : X \to X$ is a d-to-1 mapping, then the graph Γ_f might look like something going up and down d times; the real analogy to what the complex case is like is shown on the left hand side of Figure 1. The graph Γ_{f^n}, corresponding to f^n will oscillate rapidly, going up and down d^n times as in the right hand side of Figure 1. If we focus on the graph of the map, we are led to consider properties of Γ_{f^n} as $n \to \infty$. Such properties might be: (1) the area (volume) growth of Γ_{f^n} as $n \to \infty$, or (2) the number of intersection points in $\Delta \cap \Gamma_{f^n}$, where $\Delta \subset X \times X$ is the diagonal, which yields the number of fixed points of f^n. Both of these have appeal for analysts (or algebraic geometers) in the complex case because (1) the volume of a variety is easy to compute, and (2) intersection theory is well developed. Here we consider the case where $X = \mathbf{R}^2$ is the real plane, and $f : X \to X$ is rational, i.e. the coordinate functions of f are rational functions. We let $\tilde{f} : \mathbf{C}^2 \to \mathbf{C}^2$ denote the complexification of f. In fact, for a compactification $\tilde{X}$ of $\mathbf{C}^2$, $\tilde{f}$ induces a meromorphic map $\tilde{f} : \tilde{X} \to \tilde{X}$. The nth iterate of a meromorphic map is again meromorphic, and the complexification commutes with iteration, i.e. $\widetilde{(f^n)} = (\tilde{f})^n$.

In dimension 2, there is a difference between the dynamics of invertible and non-invertible maps. It is typical that a bimeromorphic map of a complex surface exhibits "saddle type" behavior, whereas a holomorphic mapping of $\mathbf{P}^2$ of topological degree $d \geq 2$ typically exhibits "expanding" behavior. Throughout this talk, we assume that f is invertible.

The map $\tilde{f}$ is holomorphic outside a finite set $I = I(f)$ of points of indeterminacy. The forward iterates f^n, $n \geq 1$ are well-defined (single-

valued) only off of the set $\bigcup_{n \geq 0} f^{-n}I$. However, the pull-back

$$f^* : H^{1,1}(\tilde{X}) \to H^{1,1}(\tilde{X})$$

is well-defined. Birational maps have a lot in common with invertible maps. They can fail to be invertible mappings in specific ways: they can blow curves down and blow up points. We will consider mappings with the property that if a curve is blown down to a point, the forward orbit of that point never gets blown up. In other words, $\bigcup_{n \geq 0} f^{-n}I$ contains no curve. In this case, $(\tilde{f}^*)^n = (\tilde{f}^n)^*$ for all $n \geq 1$, in which case we say that this compactification is natural for $H^{1,1}$. It follows that the area of $\Gamma_{\tilde{f}^n} \subset \tilde{X} \times \tilde{X}$ grows like ρ^n, where ρ is the spectral radius of f^*. Diller and Favre [DF] have shown that for any birational map $\tilde{f} : \tilde{X} \to \tilde{X}$ there is a birational equivalence $h : \hat{X} \to \tilde{X}$ and an induced birational map $\hat{f} = h^{-1}\tilde{f}h : \hat{X} \to \hat{X}$ such that $(\hat{f}, \hat{X})$ is natural for $H^{1,1}$.

The rate of volume growth of the graph of a complex mapping is closely related to the entropy of f. It is elementary that the entropy of the real map is no greater than the entropy of its complexification. By the estimate of Friedland [F], it follows that

$$entropy(f) \leq entropy(\tilde{f}) \leq \log \rho$$

where ρ denotes the spectral radius of f^*. Thus one strategy for bounding the entropy of a real rational mapping is to find a complex compactification which is natural for $H^{1,1}$.

In the sequel we focus on two families of maps. The first is

$$h_{a,b}(x, y) = (a - x^2 - by, x).$$

for $a, b \in \mathbf{R}$, $b \neq 0$, which are polynomial automorphisms. This family can take many forms under affine conjugacy: under the conjugacy $(x, y) \mapsto (-y, -x)$, it becomes

$$(x, y) \mapsto (y, y^2 - a - bx).$$

Conjugated by $(x, y) \mapsto (ax, ay)$, $h_{a,b}$ becomes

$$(x, y) \mapsto (1 - ax^2 - by, x),$$

which is the family introduced and studied numerically by Hénon [H]. The compactification $\tilde{X} = \mathbf{P}^2$ is natural for h, but $\tilde{X} = \mathbf{P}^1 \times \mathbf{P}^1$ is not. The dimension of $H^{1,1}(\mathbf{P}^2)$ is one, and $\tilde{h}^*$ acts on $H^{1,1}(\mathbf{P}^2)$ as

multiplication by 2. Thus the entropy of the real map $h_{a,b}$ is bounded above by $\log 2$ (see [FM]). The second family is

$$f_a(x,y) = (y\frac{x+a}{x-1}, x+a-1)$$

for $a \in \mathbf{R}$. This family was studied extensively from the computational point of view in [AABHM1,2,3] and [AABM1,2]. The compactification $\tilde{X} = \mathbf{P}^1 \times \mathbf{P}^1$ is natural for f_a if $a \neq 1/n$, for $n \geq 1$ and $a \neq n/(n+2)$, for $n \geq -1$. (On the other hand, the compactification $\tilde{X} = \mathbf{P}^2$ is not natural for f_a.) The action of f^* on $H^{1,1}(\mathbf{P}^1 \times \mathbf{P}^1)$ is given by $\begin{pmatrix} 0 & 1 \\ 1 & 1 \end{pmatrix}$. The spectral radius of f^* is $(1+\sqrt{5})/2$, and so the entropy of f_a is no greater than $\log((1+\sqrt{5})/2)$.
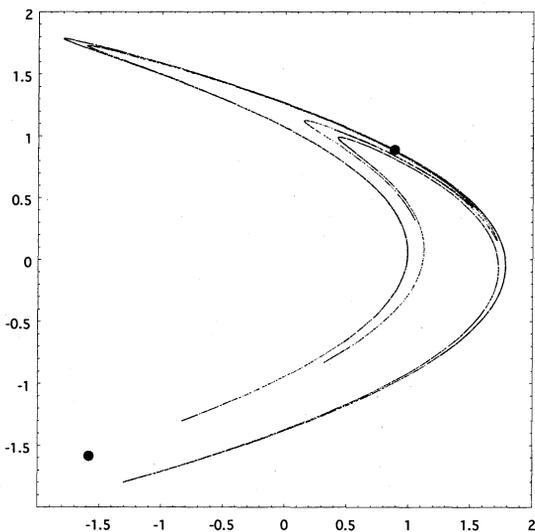

Figure 2. Orbit portrait for $h_{a,b}$: $a = 1.4$, $b = -.3$

§1. Polynomial Diffeomorphisms of $\mathbf{R}^2$

We will compare the real and complex points of view on dynamical systems by contrasting the sorts of computer pictures that may be drawn. Computer pictures that are well planned and executed have been a powerful tool for the development of dynamical systems. One frequently drawn picture is that of an orbit portrait: given a point $p \in \mathbf{R}^2$,

one plots the forward orbit $O^+(p) = \{f^n p : n \geq 0\}$. Sometimes an orbit portrait $O^+(p)$ is interesting and sometimes it is not, as in the case when $f^n p$ converges to a sink (or to infinity) as $n \to \infty$. The pictures in [H], [AABHM1,2,3] and [AABM1,2] are point orbits, as well as Figure 2, which plots the first 10000 iterates of a point. The large dots are the two (fixed) saddle points of h. This map will be discussed further in §4.
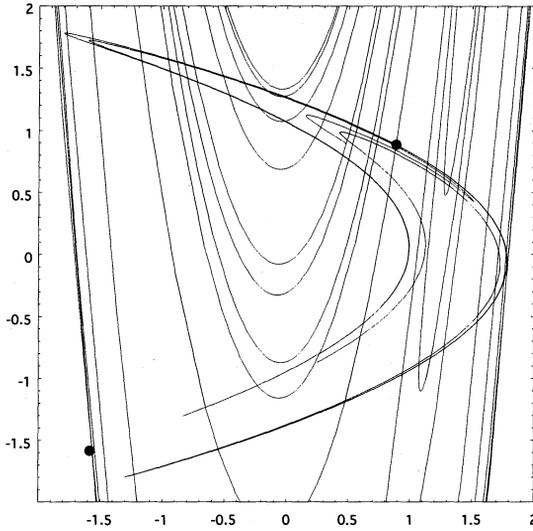

Figure 3. Stable/unstable manifolds for upper right hand fixed point: $a = 1.4$, $b = -.3$
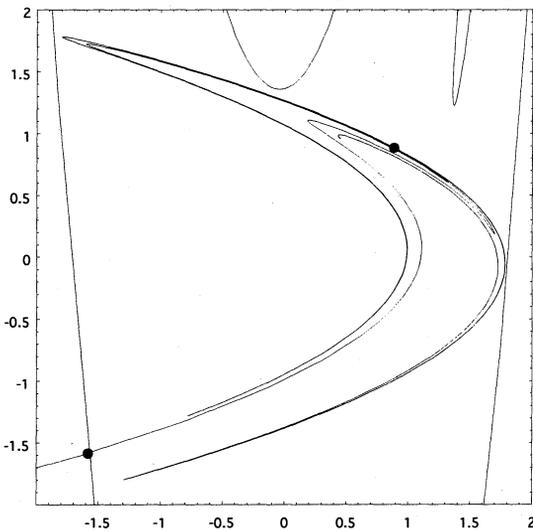

Figure 4. Stable/unstable manifolds for lower left hand fixed point: $a = 1.4$, $b = -.3$

A point p is a saddle fixed point if $h(p) = p$ and the eigenvalues λ^s and λ^u of $h'(p)$ satisfy $0 < |\lambda^s| < 1 < |\lambda^u|$. Then there are stable and unstable manifolds $W^s(p)$ and $W^u(p)$ passing through p. A useful computer picture is to show $W^{s/u}(p)$ directly, or more precisely, to draw a large arc inside $W^s(p)$ and a large arc inside $W^u(p)$.

Figure 3 corresponds to the same mapping as Figure 2. We have chosen p to be the upper right hand saddle point (indicated by the dot), and we have drawn an arc of length about 40 inside $W^u(p)$. This unstable arc closely resembles the orbit portrait in Figure 2. We have also drawn a considerably longer subarc of $W^s(p)$. While this arc is connected, it is cut off by the viewbox, and the resulting picture resembles a number of parabolas opening upward.

Figure 5 arises from a horseshoe mapping. The saddle point $p = (-4, -4)$ is indicated by the dot. The pieces of curves which look like parabolas opening to the left are all part of a (connected) arc of $W^u(p)$, which is clipped off by the viewbox. The pieces which resemble parabolas opening downwards are portions of an arc inside $W^s(p)$. One property of the horseshoe is that it is hyperbolic; the apparent transverse intersection of $W^s(p)$ and $W^u(p)$ is consistent with this. Another property is that if p_1 and p_2 are saddles, then $W^s(p_1)$ and $W^s(p_2)$ have the same closures. Thus we do not need to draw $W^{s/u}$ for the other saddle fixed point.
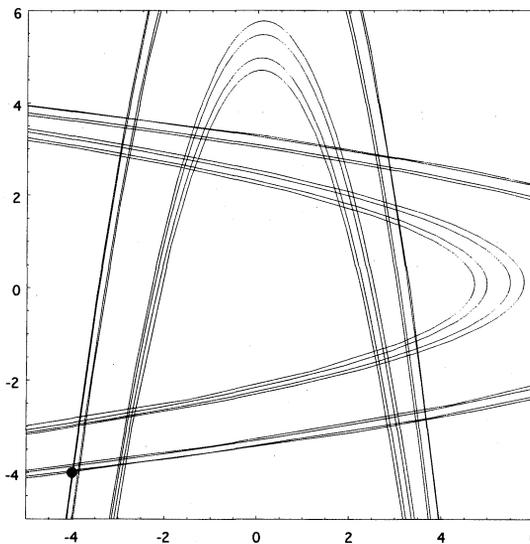

Figure 5. Stable and unstable manifolds of $h_{a,b}$: $a = 8$, $b = 1$

In order to describe pictures in $\mathbf{C}^2$ we need to first develop some knowledge about the situation in the complex domain and what we might hope to see of dynamical significance. Let us define the rate of escape functions

$$G^{\pm}(x,y) = \lim_{n \to \infty} \frac{1}{2^n} \log^+ |\tilde{h}^{\pm n}(x,y)|$$

which give the super-exponential rate of escape to infinity of the orbit of a point (x,y) in forward/backward time. These functions are psh and continuous on $\mathbf{C}^2$, and $G^{\pm}$ is pluriharmonic on $\{G^{\pm} > 0\}$. It is evident that $G^{\pm}$ satisfies $G^+ \circ \tilde{h} = 2G^+$ and $G^- \circ \tilde{h} = \frac{1}{2}G^-$. We set $K^{\pm} = \{G^{\pm} = 0\}$ and $K = K^+ \cap K^-$ and $J^{\pm} = \partial K^{\pm}$, and $J = J^+ \cap J^-$.

Figure 6[2] uses the same real viewbox $[-2,2] \times [-2,2]$ as Figures 2, 3 and 4. The white/gray/black regions are the sets $\{c_1 < G^- < c_2\}$, and under h such a region is mapped in to $\{\frac{c_1}{2} < G^- < \frac{c_2}{2}\}$. The set K^- has zero area and is not directly visible. It is detected indirectly: to reach a point of K^-, it is necessary to pass through an infinite number of color transitions.
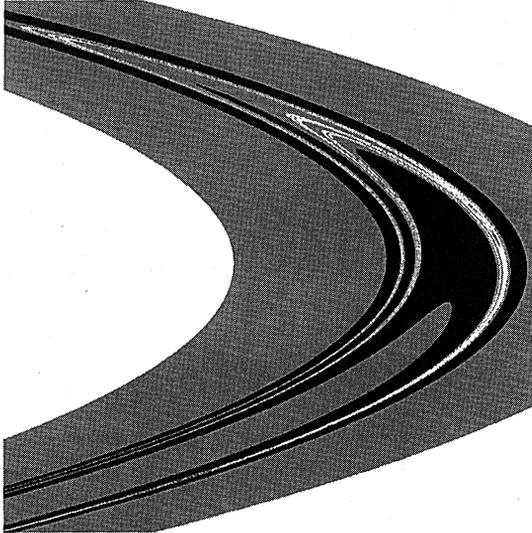

Figure 6. Level sets of G^- in $\mathbf{R}^2$ closing down on $K^- \cap \mathbf{R}^2$: $a = 1.4$, $b = -.3$

---

[2]Figure 6 and all the unstable slice pictures were made using the program FractalAsm which was developed by J.H. Hubbard and K. Papadantonakis. This program and other useful dynamical software is freely available at http://www.math.cornell.edu/~dynamics. The algorithms are explained in detail in [HP].

We define the currents $\mu^{\pm} = \frac{1}{2\pi}dd^cG^{\pm}$; they satisfy $\tilde{h}^*\mu^+ = 2\mu^+$ and $\tilde{h}^*\mu^- = \frac{1}{2}\mu^-$, and $J^{\pm} = \text{supp}(\mu^{\pm})$. Ruelle and Sullivan [RS] showed generally that if h is Axiom A, then there are invariant currents $T^{\pm}$ in $\mathbf{R}^2$. The family of stable manifolds forms a lamination $\mathcal{W}^s$, and the current T^+ is constructed from this laminar structure: it involves currents of integration over pieces of stable manifolds and a family of transversal measures to $\mathcal{W}^s$. In order to turn a manifold into a current of integration, it is necessary to choose an orientation. In the absence of some condition like hyperbolicity, the stable/unstable manifolds may do a lot of "folding", and choosing an orientation presents a problem.

The stable/unstable manifolds $W^{s/u}(p,\tilde{h})$ of $\tilde{h}$ in $\mathbf{C}^2$ are Riemann surfaces which are complexifications of $W^{s/u}(p,h) \subset \mathbf{R}^2$. When $\tilde{h}$ is Axiom A, and $K \subset \mathbf{R}^2$, it follows that $\mu^{\pm}$ is the complexification of $T^{\pm}$, that is the currents $\mu^{\pm}$ may be constructed the same as $T^{\pm}$, except that the currents of integration over pieces of the laminations $\mathcal{W}^{s/u}$ are replaced by their complexifications.

The following result, which applies to all mappings $\tilde{h}_{a,b}$, shows that $\mu^{\pm}$ may be considered in some sense to be the current of integration defined by $W^{s/u}(p,\tilde{h})$. It also shows that $W^{s/u}(p,\tilde{h})$ are imbedded in $\mathbf{C}^2$ in a complicated, non-proper way.
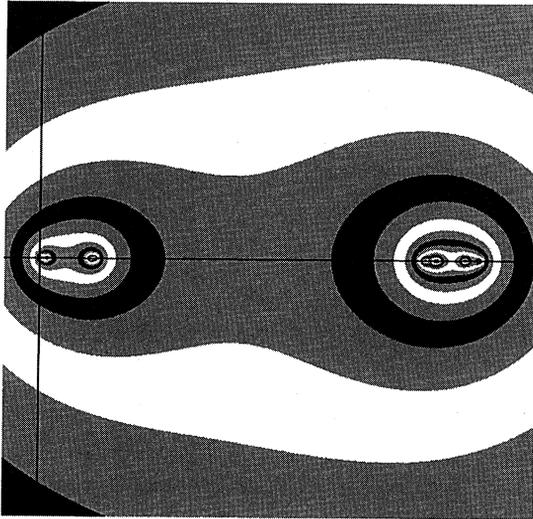

Figure 7. Unstable (complex) slice of K^+ for the horseshoe $a = 8$, $b = 1$
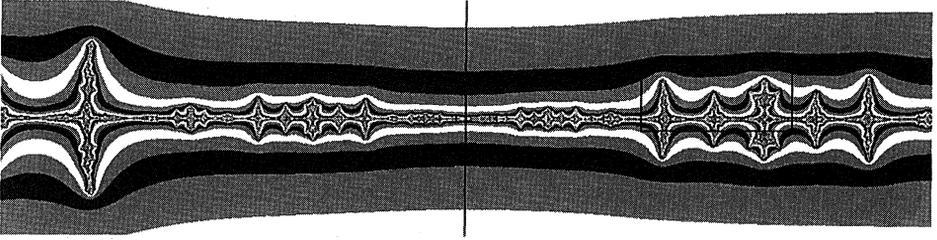
Figure 8. Level sets for G^+ for an unstable slice:[3] $a = 1.4$, $b = -.3$

Theorem ([BS1]). *Let $D^u \subset W^u(p, \tilde{h})$ denote an open disk containing p such that the current μ^+ puts no mass on ∂D^u. Then there is a constant $c > 0$ such that the normalized currents of integration $\frac{1}{2^n}[f^n D^u]$ converge to $c\mu^-$ as $n \to \infty$. It follows that for any saddle point p, the closure of $W^u(p, \tilde{h})$ is exactly J^-.*

$W^u(p, \tilde{h})$ is parametrized by an entire mapping $\psi : \mathbf{C} \to W^u(p, \tilde{h}) \subset \mathbf{C}^2$ such that $\psi(0) = p$ and $\tilde{h}(\psi(\zeta)) = \psi(\lambda^u \zeta)$ for all $\zeta \in \mathbf{C}$. (See [MNTU, §6.4].) The mapping ψ may be generated as follows. Let $v \in \mathbf{R}^2$ be an unstable eigenvector for $h'(p)$, and let $L(\zeta) = p + \zeta v$ be a parametrization of the complex line passing through p in the direction v, and

$$\psi(\zeta) = \lim_{n \to \infty} \tilde{h}^n(L((\lambda^u)^{-n}\zeta)),$$

which may be used as a naive algorithm for computing ψ. An object which is dynamically meaningful is the "unstable slice" $W^u(p) \cap K^+$. Let us define $g = G^+ \circ \psi$ which is subharmonic on $\mathbf{C}$. The most useful computer pictures have been those following an idea suggested by Hubbard: Plot the level surfaces of g and its harmonic conjugate g^* inside the plane $\mathbf{C}$.[4] Note that the set $\{g = 0\}$ corresponds to the unstable slice $W^u(p) \cap K^+$. The coloring in the Hubbard picture may be chosen so that it is self-similar under the multiplication $\zeta \mapsto \lambda^u \zeta$, since $\{g = c\}$ is taken to $\{g = 2c\}$. The picture is also symmetric under complex conjugation $\zeta \mapsto \bar{\zeta}$ because h has real coefficients. By the minimum principle for harmonic functions, every compact component of the sub-level set $\{g \leq c\}$ must intersect $\{g = 0\}$. In contrast, a linear slice such as Figure

---

[3]We are grateful to S. Ushiki for giving us a number of pictures of complex slices of this mapping in 1993.

[4]While we do not use g^* in the pictures below, the use of g^* is related to other interesting structures, in particular "external rays," see [BS6] and [O].

6 is not self similar. And for a real linear slice such as Figure 6, g is not subharmonic.
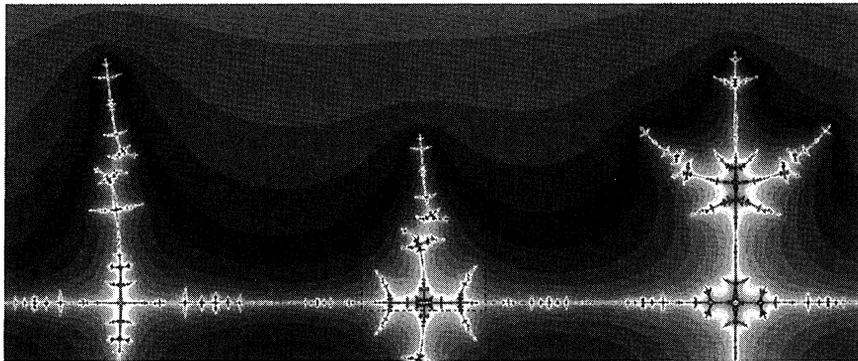

Figure 9. Detail of Figure 8, with different coloring

An example of such a picture is given in Figure 7. This is the complexification of Figure 5 inside a (square) complex disk D with $p \in D \subset W^u(p, \tilde{h})$, where p is located at the large dot in Figure 5. The origin corresponds to p under the map ψ, and the x-axis corresponds to the interval of $W^u(p)$ running from about $x = -4.5$ to about $x = -2$. That is, D cuts through the left hand legs of all the downward-opening parabolas. It appears that the points of $K^+ \cap W^u(p)$ lie on the x-axis, which corresponds to the property of the real horseshoe that $K \subset \mathbf{R}^2$.

Figure 8 gives the complex slice by the complexification of the unstable manifold in Figure 3. The origin is at the exact center of the picture (the imaginary axis has been drawn in) and the origin corresponds (under ψ) to p. The x-axis in Figure 8 corresponds in Figure 3 to a relatively short arc of $W^u(p)$ containing p. An interesting feature here is that there are "limbs" which rise off of the x-axis. This corresponds to the intersection between the Riemann surface $W^u(p, \tilde{h})$ and points of K^+ lying outside of $\mathbf{R}^2$. It is intriguing to know whether there is any connection between the "limbs" and the stable/unstable intersections in Figure 3.

Figures 9 and 10 give successively more detailed blow-ups of Figure 8. Note that the scheme for coloring the level sets $\{2^{-n-1} < G^+ < 2^{-n}\}$ has been changed, giving a different visual impression of $W^u(p) \cap K^+$. Figures 9 and 10 make it clear that the unstable slice contains a compact component. By [BS2] this implies that $J \subset \mathbf{C}^2$ is disconnected.
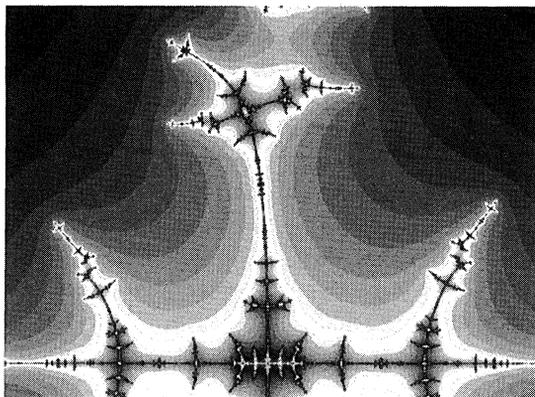
Figure 10. Detail of Figure 9

§2. Horseshoes and Maps of Maximal Entropy

We say that h has maximal entropy if $entropy(h) = \log 2$. Real mappings of maximal entropy are especially well suited for treatment by complex methods. Recall that by [FM] the entropy is equal to the exponential rate of growth of periodic points:

$$entropy(h) = \lim_{n \to \infty} \left(\#\{p \in \mathbf{R}^2 : h^n(p) = p\} \right)^{\frac{1}{n}}.$$

The situation is simpler, or at least more complete, in the complex domain. By the Bezout Theorem (see [FM]), we have that $\#\{p \in \mathbf{C}^2 : h^n(p) = p\} = 2^n$, counting multiplicity. It was shown in [BLS] that h has maximal entropy if and only if $\{p \in \mathbf{C}^2 : h^n(p) = p\} \subset \mathbf{R}^2$ holds for all $n \geq 1$.

The Smale horseshoe mapping is an important mapping which arises in many situations. Let us describe the horseshoe from the topological point of view. We start with a homeomorphism $f : \mathbf{R}^2 \to \mathbf{R}^2$, and we suppose that there is a topological box $B \subset \mathbf{R}^2$ which is mapped across itself as in the left hand side of Figure 11.
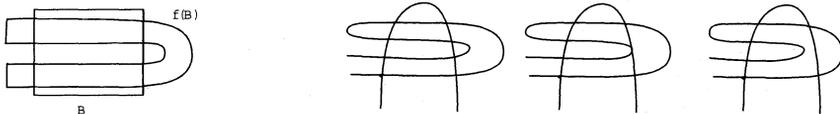

Figure 11. Topological horseshoe and degeneration

Let us define

$$B_\infty = \{p \in B : f^n p \in B, \ \forall n \in \mathbf{Z}\}.$$

Thus $f : B_\infty \to B_\infty$ is the dynamical system within B that is induced by f. Let us choose an arbitrary labeling of the the components of $B \cap fB$ by "0" and "1". We give the set $\{0, 1\}$ the discrete topology and we give the sequence space $\Sigma = \{0, 1\}^{\mathbf{Z}}$ the infinite product topology. We let $c : B_\infty \to \Sigma$ be the coding map where $c(p)$ is the itinerary of the orbit of p. That is, $c(p) = \cdots c_{-1} c_0 c_1 \cdots$ is an infinite sequence of 0's and 1's, where the nth symbol is determined by the condition that $c_n = 0$ if $f^n(p) \in B_0$, and $c_n = 1$ if $f^n(p) \in B_1$. We define the shift map as $\sigma(c) = c'$, where $c' = \cdots c'_{-1} c'_0 c'_1 \cdots$ is given by $c'_n = c_{n+1}$. Thus σ induces a dynamical system on Σ. It is evident, then, that the map c induces a semi-conjugacy from the dynamical system (f, B_∞) to (σ, Σ).

The standard treatment of the horseshoe is to assume at this stage that f is hyperbolic on B_∞, which is to say that there is a splitting of the tangent space $T_p \mathbf{R}^2 = E_p^s + E_p^u$, $p \in B_\infty$ into subspaces which are uniformly contracted/expanded under f'. It follows from the contraction/expansion, that the connected components of $B \cap f^{-n} B \cap f^n B$ shrink to points as $n \to \infty$. Thus the coding map $c : (f, B_\infty) \to (\sigma, \Sigma)$ is in fact a conjugacy. The horseshoe map (f, B_∞) has an interesting geometry arising from its imbedding in $\mathbf{R}^2$ (see Figure 5) and it has a simple symbolic model, which is the topological analogue of the Bernoulli shift model of coin flipping.

It was discovered by Hubbard and Oberste-Vorth [HO] (see also [MNTU, §7.4]) that if the map $f = h_{a,b}$ and a square $B = \{(x, y) \in \mathbf{R}^2 : |x|, |y| < R\}$ generate a topological horseshoe, then hyperbolicity follows automatically (by use of the Poincaré metric on a complex neighborhood). The definition of horseshoe given above specifies a method of construction. Let us give a more general definition in terms of dynamical properties alone. We say that a mapping $h_{a,b}$ is a complex horseshoe if $\tilde{h}_{a,b}$ is hyperbolic on K, and $(\tilde{h}_{a,b}, K)$ is topologically conjugate to the 2-shift (σ, Σ). The complex horseshoes are widespread: Hubbard and Oberste-Vorth (see [MNTU, §7.4]) showed that $\tilde{h}_{a,b}$ generates a complex horseshoe if $|a| > 2(1 + |b|)^2$.

We would like to use the horseshoes as a starting place to explore what is happening in parameter space $\mathcal{P} = \{(a, b) \in \mathbf{R}^2 : b \neq 0\}$. A complex horseshoe is said to be a real horseshoe (or simply a horseshoe) if $K \subset \mathbf{R}^2$. We define the horseshoe locus $\mathcal{H} \subset \mathcal{P}$ to be the set of parameters such that $h_{a,b}$ is a (real) horseshoe. Note that the entropy of a horseshoe is $\log 2$, and $(a, b) \mapsto entropy(h_{a,b})$ is a continuous func-

tion, so that the closure $\bar{\mathcal{H}}$ of $\mathcal{H}$ in $\mathcal{P}$ consists of mappings of maximal entropy. If $(a_0, b_0) \in \mathcal{P}$ is a parameter for which f_{a_0, b_0} is hyperbolic, then $(f_{a,b}, J_{a,b})$ is conjugate to $(f_{a_0,b_0}, J_{a_0,b_0})$ for (a, b) sufficiently close to (a_0, b_0). If f_{a_0, b_0} is not hyperbolic, then there is no general statement about nearby maps.

Let us consider $(a_0, b_0) \in \partial \mathcal{H}$ in the boundary of the horseshoe locus. This mapping is not hyperbolic. There are several possible ways that hyperbolicity might break down. One of them is that the uniformity of the expansion or contraction is lost. However, if h is a mapping of maximal entropy, then every saddle point p of period n is uniformly hyperbolic: the multipliers of $Dh^n(p)$ satisfy $|\lambda^s| \leq 2^{-n}$ and $|\lambda^u| \geq 2^n$. (See [BS3] for details.) Thus the uniformity of expansion and contraction is maintained to the boundary of $\mathcal{H}$. The way that horseshoes of the form $h_{a,b}$ can degenerate is pictured in the right hand side of Figure 11: a loop of unstable manifold "pulls through" to create a tangency. That is, the picture on the left hand side of the triplet corresponds to a horseshoe; the central picture corresponds to $\partial \mathcal{H}$; and by the right hand picture we have completely left $\bar{\mathcal{H}}$. This picture is summarized in the following:

Theorem [BS4]. *Suppose that $b > 0$ and $h_{a,b}$ is a mapping of maximal entropy. Then either $h_{a,b}$ is hyperbolic, or there is a point of tangential intersection between $W^u(p_+)$ and $W^s(p_+)$, where p_+ denotes the unique fixed point such that the eigenvalues of $Df(p_+)$ are both positive.*

We can extend this result to a more global description of $\mathcal{H}$.

Theorem [BS5]. *There are real analytic functions κ^+ and κ^- defined on the interval $[-.085, .085]$ such that*
(1) $\mathcal{H} \cap \{|b| < .085\} = \{(a, b) \in \mathcal{P} : a > \max(\kappa^+(b), \kappa^-(b))\}$.
(2) If $a < \max(\kappa^+(b), \kappa^-(b))$, $0 < |b| < .085$, then $entropy(h_{a,b}) < \log 2$.

This shows that the horseshoe locus is nicely bounded by two real analytic curves, at least in the region $|b| < .085$. The bifurcation situation on the other side of $\partial \mathcal{H}$ is very complicated: some of this complexity is suggested by the computer picture in El Hamouly and Mira [EM].

§3. A Family of Birational Maps

Let us describe the birational map f_a of $\mathbf{R}^2$ to itself. We consider the complex compactification $\mathbf{P}^1 \times \mathbf{P}^1$. Intersecting this with the real points,

we have f_a on the torus $S^1 \times S^1$. The mapping f_a has a rational inverse. In fact, f_a is conjugate to f_a^{-1} via the involution $\tau(x, y) = (-y, -x)$. However, if $a \neq -1$, f_a is not a diffeomorphism: its critical locus is $\mathcal{C} = \{x = 1\} \cup \{x = -a\}$. The line $\{x = 1\}$ is mapped to the point (∞, a). The points of indeterminacy are $(1, 0)$ and $(-a, \infty)$. One of the fixed points is (∞, ∞), which is parabolic, and so f_a is not hyperbolic. The other fixed point is $p_a = ((1 - a)/2, (a - 1)/2)$. If $a < 0$, $a \neq -1$, then p_a is a saddle point. If $a = -2$, then the saddle point is $(3/2, -3/2)$; an arc inside its unstable manifold is given in Figure 12. We are working on the torus, so the bands of curves that exit to the right through the vertical line $x = 20$ continue on in $S^1 \times S^1$ through $\{x = \infty\} \times S^1$ and then re-enter the picture from the left through $x = -20$. The two critical lines are indicated as dotted vertical lines. Let Γ denote the set of all of the arcs which pass between the components of $\mathcal{C}$. Since $f_a(\{x = 1\}) = (\infty, a)$, and $f_a(\{x = -a\}) = (0, -1)$, it follows that $f(\Gamma)$ is the topmost band of arcs in Figure 12, running from $(0, -1)$ (where they are pinched together) to $(\infty, a) = (\infty, -2)$ (where they are also pinched together). This pinching phenomenon does not occur for diffeomorphisms.

The orbit of $(0, -1)$ marches off to infinity: $f^n(0, -1) = (na, na - 1)$. The "pinched" point $(0, -1)$ and its orbit of pinches $(-2, -3)$, $(-4, -5)$, etc., are visible in Figure 12. Similarly, the orbit of (∞, a) goes to (∞, ∞) along pinch points, alternating between $\{x = \infty\}$ and $\{y = \infty\}$.

Since f_a is conjugate to its inverse via the involution τ, we could obtain a picture of the stable manifold by applying τ to Figure 12, i.e., flipping it about the line $y = -x$.

The approach we have taken in [BD1] is first to work in the category of complex dynamics. The map induced on $H^{1,1}$ is given by $f^* = \begin{pmatrix} 0 & 1 \\ 1 & 1 \end{pmatrix}$, which has $\lambda = (1 + \sqrt{5})/2$ as its spectral radius. There are invariant currents $\mu^\pm$ with the property that $\tilde{f}^* \mu^\pm = \lambda^{\pm 1} \mu^\pm$. The current μ^- is given by the unstable manifold, and Figure 12 gives a good picture of what the real slice of μ^- looks like for $a = -2$.
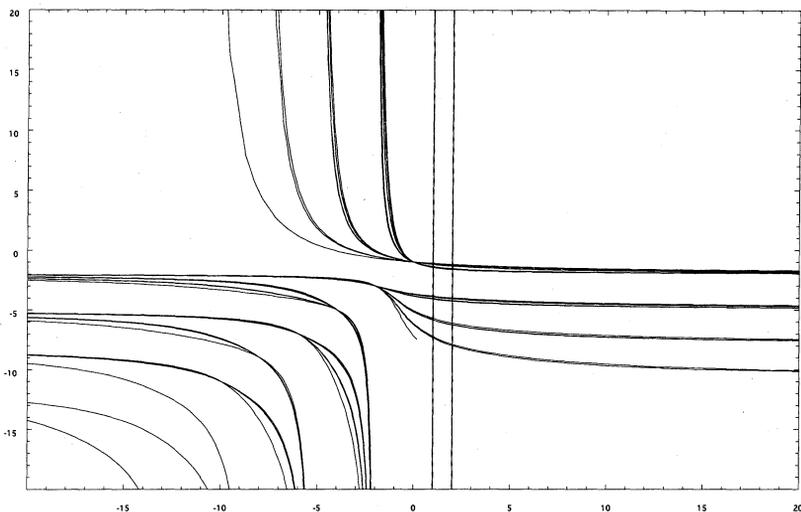
Figure 12. Unstable manifold for f_a: $a = -2$

We would also like to take the wedge product $\mu := \mu^+ \wedge \mu^-$ and obtain an invariant measure. Although the local potentials of μ^+ and μ^- are both unbounded near (∞, ∞), the wedge product may be defined (see [BD2]). Given the laminar structure of μ^+ and μ^-, the wedge product coincides with the intersection product. To help visualize the measure μ in the case $a = -2$, we have re-drawn $W^u(p_a)$ in Figure 13, together with $W^s(p_a)$, which is its "flip" under τ: μ is a measure carried by the intersection of these two sets. Further general properties of μ are that it is mixing, and the larger Lyapunov exponent is bounded below by $\frac{1}{8} \log \lambda > 0$.

The measure μ plays the same basic role in the dynamics of $\tilde{f}_a$ that the measure μ plays for the mappings $\tilde{h}_{a,b}$. Our plan is to show that if $a < 0$, $a \neq -1$, then μ puts no mass on $\mathbf{P}^1 \times \mathbf{P}^1 - \mathbf{R}^2$. We may obtain μ^+ (resp. μ^-) by pulling back the current of integration over a vertical line L (resp. pushing forward the current of integration over a horizontal line L):

$$\mu^\pm = \lim_{n \to \infty} \frac{1}{\lambda^n} f^{\pm n *}[L] = \lim_{n \to \infty} \frac{1}{\lambda^n} [f^{\mp n} L]$$

We know that f^* is represented by the matrix $\begin{pmatrix} 0 & 1 \\ 1 & 1 \end{pmatrix}$, and the entries of the nth power of this matrix are the Fibonacci numbers. Thus we know that the number of complex intersections $f^n\{y = const\} \cap f^{-m}\{x = const\}$ is given by Fibonacci numbers.

Now we require that $a < 0$, $a \neq -1$. We show by a combinatorial/geometric argument that for $c_1 > 1$, $c_2 < -1$, the number of points in $f^n\{y = c_2\} \cap f^{-m}\{x = c_1\} \cap \mathbf{R}^2$ is given by these same Fibonacci numbers. Thus all of the complex intersections $f^n\{y = c_2\} \cap f^{-m}\{x = c_1\}$ are simple and occur already in $\mathbf{R}^2$. Using the Lefschetz Index Theorem, we get an exact count of the points of period n, and we conclude that (except for the point (∞, ∞)) the fixed points all lie in $\mathbf{R}^2$ and are saddles.
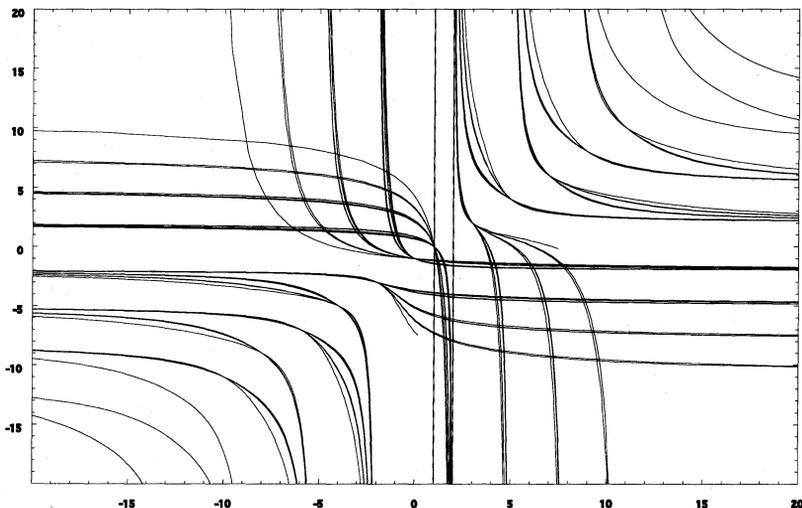

Figure 13. Intersection of stable/unstable laminations produces invariant measure

Further, for almost every $c_1 > 1$ and $c_2 < -1$, we have

$$\mu = \lim_{n \to \infty} \frac{1}{\lambda^{2n}} [f^n\{y = c_2\} \cap f^{-m}\{x = c_1\}]$$

where the right hand side means that the measure is defined by the sum of the point masses at the intersection points.

Now let $\Omega \subset \mathbf{R}^2$ denote the support of μ. Let R_0 denote the fourth quadrant and R_1 denote the second quadrant. We show that $\Omega \subset R_0 \cup R_1$ and $f_a(R_1 \cap \Omega) \cap R_1 = \emptyset$. Let Σ_G denote the so-called "golden mean" subshift of Σ, which consists of the set of bi-infinite symbol sequences of 0's and 1's such that 1 is always followed by 0, which is to say that the word "11" does not appear anywhere in the sequence. The shift $\sigma : \Sigma_G \to \Sigma_G$ defines a dynamical system, and there is a unique invariant measure η of entropy $\log \lambda$.

We let $c : \Omega \to \Sigma_G$ be the coding map, which sends a point p to its itinerary, just as we did in the case of the horseshoe. This coding map is well-defined outside the zero measure set of points whose orbits contain the point of indeterminacy $(-a, \infty)$ for f or the point of indeterminacy (∞, a) for f^{-1}. It follows that c gives a measure-theoretic equivalence between (Ω, μ) and (Σ_G, η). Thus the real map f_a has maximal entropy since (Σ_G, η) has entropy $\log \lambda$.

§4.   The Hénon Attractor

Hénon [H] performed numerical explorations of the family $\{h_{a,b}\}$ from the point of view of finding dynamical phenomena. One mapping he focused on is $h = h_{a,b}$ with $a = 1.4$ and $b = -.3$. The study of this mapping has led to "computer phenomena" which have given rise to an area rich with questions and conjectures. Deep results have been obtained (see Benedicks and Carleson [BC]), but interestingly enough they seem not to be applicable to these parameters. In fact, it seems unclear what the phenomena might actually be. Perhaps a reconsideration of these questions in the complex domain will lead to formulations which can be understood and proved.

In Figures 2, 3, and 4, we have seen an orbit portrait and pairs of stable/unstable manifolds for h. Figure 3 suggests that $W^s(p)$ and $W^u(p)$ have transverse intersection points, and thus h has positive entropy. Since h has a nonreal periodic point $p \in \mathbf{C}^2 - \mathbf{R}^2$ (for instance, there is one of period 3), it follows from [BLS] that the entropy of h is strictly less than $\log 2$.

Hénon showed that there is a quadrilateral $Q \subset \mathbf{R}^2$ with the property that $h(\bar{Q}) \subset int(Q)$. Thus $A := \bigcap_{n \geq 0} h^n(Q)$ is an attractor in the sense of Conley. (There are several reasonable definitions of "attractor.") If we set $B := \bigcup_{n \geq 0} h^{-n}(Q)$, then the orbit of every point of B approaches A in forward time in the sense that $\lim_{n \to \infty} dist(h^n q, A) = 0$ for all $q \in B$. An additional feature that one would like to ask for the attractor A would be minimality.

Let us use p_R (resp. p_L) to denote the upper right hand (resp. lower left hand) fixed point of h. All unstable manifolds (and their complexifications) are contained in K^-, so $\overline{W^u(p_L)} \subset K^- \cap \mathbf{R}^2$. It is easy to imagine that $\partial B = W^s(p_L)$. Since p_R is contained in the quadrilateral Q, it follows that

$$\overline{W^u(p_R)} \subset A \subset K \cap \mathbf{R}^2.$$

Thus $W^u(p_R)$ is contained in the basin B, so $W^u(p_R)$ is contained in the interior of K^+ inside $\mathbf{R}^2$. On the other hand, saddle points (and in

particular p_R) never belong to the $\mathbf{C}^2$-interior of K^+. In Figure 8 we
see that 0 is not even in the interior of the unstable slice (because the
picture is self-similar about 0).

If we remove p_L, the unstable manifold splits into two pieces $W^u(p_L) - \{p_L\} = \gamma' \cup \gamma''$, where γ' (resp. γ'') is the part which leaves p_L in the
lower left (resp. upper right) direction. Figure 14, the complex unstable
slice, can be used to prove that $\gamma' \cap K^+ = \emptyset$, by showing that G^+ is
strictly positive in a fundamental region of the negative x-axis. On the
other hand Figure 14 is consistent with the idea that $\gamma'' \subset K^+$. Since
$p_L \notin Q$ and p_L is fixed, we have $p_L \notin B$, so

$$W^u(p_L) \cap A = \emptyset.$$

Let us define the ω-limit set, written $\omega(q)$, of a point q to be the set of
accumulation points of the forward orbit $O^+(q)$. One device for plotting
a computer picture of $\omega(q)$ is to plot the set $\{h^j(q) : n_1 \leq j \leq n_2\}$.
Choosing n_1 large would remove extraneous points of $O^+(q)$ and allow
$h^j(q)$ time to get close to $\omega(q)$. Choosing n_2 large would give enough
points to "fill out" $\omega(q)$. In Figure 2, we chose q rather close to $\omega(q)$, so
that $O^+(q)$ is close to $\omega(q)$.

An intriguing computer phenomenon discovered in [H] is that for
"every" point $p \in Q$, the computer picture of $\omega(p)$ looks the same.
This gives computer evidence that there is a compact set $\Omega \subset \mathbf{R}^2$ such
that $\omega(p) = \Omega$ for almost every $p \in B$. For the sake of discussion, let us
suppose that such an Ω exists, and let us write $B' = \{p \in B : \omega(p) = \Omega\}$.
It is easy to see that

$$\Omega \subset A, \text{ and } W^s(p_R) \cap B' = \emptyset.$$

In fact, if we draw more and more of $W^s(p_R)$ it starts to look as though
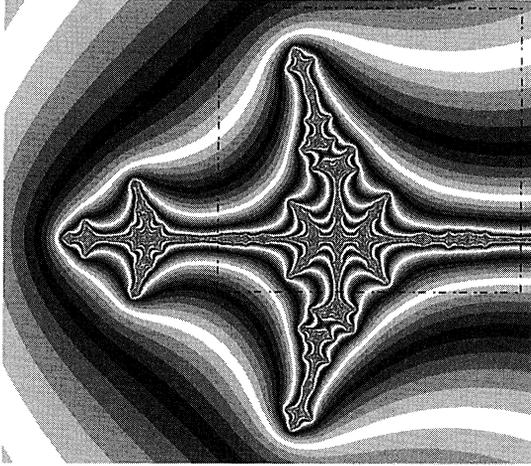the stable manifold could be dense in B.

Figure 14. Unstable (complex) slice for lower left saddle point: $a = 1.4$, $b = -.3$

An inspection of Figures 2 and 3 seems to suggest that $\overline{W^u(p_R)} = \Omega$. On the other hand, this may be a case where the computer picture is deceptive: any differences between them may only become visible at a very small scale. Let us point out that $W^u(p_L)$ also looks very much like Ω, but we have $W^u(p_L) \cap \Omega \subset W^u(p_L) \cap A = \emptyset$.

One question that has been studied is whether A contains a sink orbit (a situation in which A would not be minimal). In fact, it has not been possible to prove that Ω itself is not a sink orbit, which would necessarily have a high period. A celebrated result of Newhouse and Robinson states that if f_t is a family of mappings with a nondegenerate tangency, then there is an interval $[\alpha, \beta]$ and a residual set $T \subset [\alpha, \beta]$ such that for $t \in T$, f_t has infinitely many sinks. (The possibility of a tangency is consistent with Figure 3.) Fornæss and Gavosto [FG1,2] have shown that the family $g_t = h_{1.395,t}$ is nondegenerate in a neighborhood of $t = -.3$, and so there is such an interval $[\alpha, \beta]$ containing $-.3$ in its interior.

Let us note that this region of parameter space is rich with bifurcations, and the point $(1.395, -.3)$ would not be considered to be "close" to $(1.4, -.3)$, in the sense that the dynamical system $h_{1.395,-.3}$ is separated from h by infinite cascades of bifurcations. On the other hand, the computer phenomenon of the Hénon attractor is robust in the sense that $h_{1.395,-.3}$ generates an attractor with the same appearance as A.

Now suppose that h has an attracting periodic point q. Let $\mathcal{B}$ denote the basin of attraction of q in $\mathbf{C}^2$. It is a theorem that $\partial \mathcal{B} = \partial K^+$, and $\mathcal{B}$ intersects any (complex) algebraic curve. In particular, it intersects

any complex line. We do not know whether in fact $\mathcal{B}$ can exist, but the various unstable slice pictures indicate that the intersection $W^u \cap \mathcal{B}$ must be small.
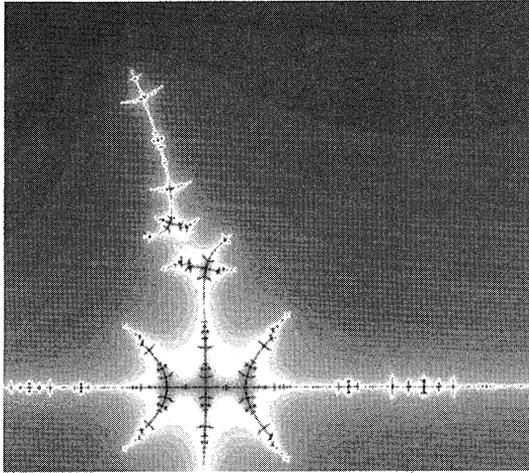

Figure 15. Detail of Figure 14

References

[AABHM1]   N. Abarenkova, J.-Ch. Anglès d'Auriac, S. Boukraa, S. Hassani and J.-M. Maillard, Rational dynamical zeta functions for birational transformations, Physica A, **264** (1999), 264–293.

[AABHM2]   N. Abarenkova, J.-Ch. Anglès d'Auriac, S. Boukraa, S. Hassani and J.-M. Maillard, Topological entropy and complexity for discrete dynamical systems, Phys. Lett. A, **262** (1999), 44–49.

[AABHM3]   N. Abarenkova, J.-Ch. Anglès d'Auriac, S. Boukraa, S. Hassani and J.-M. Maillard, Growth complexity spectrum of some discrete dynamical systems, Physica D, **130** (1999), 27–42.

[AABM1]   N. Abarenkova, J.-Ch. Anglès d'Auriac, S. Boukraa and J.-M. Maillard, Real Arnold complexity versus real topological entropy for birational transformations, J. Phys. A., **33** (2000), 1465–1501.

[AABM2]   N. Abarenkova, J.-Ch. Anglès d'Auriac, S. Boukraa and J.-M. Maillard, Real topological entropy versus metric entropy for birational measure-preserving transformations, Physica D, **144** (2000), 387–433.

[BD1]   E. Bedford and J. Diller, The dynamics of a family of birational maps of the plane.

[BD2]   E. Bedford and J. Diller, Energy and invariant measures for birational surface maps.

[BLS]   E. Bedford, M. Lyubich, and J. Smillie, Polynomial diffeomorphisms of $\mathbf{C}^2$: IV. The measure of maximal entropy and laminar currents, Invent. Math., **112** (1993), 77–125.

[BS1]   E. Bedford and J. Smillie, Polynomial diffeomorphisms of $\mathbf{C}^2$ II: Stable manifolds and recurrence, J. Amer. Math. Soc., **4** ((1992), 657–679.

[BS2]   E. Bedford and J. Smillie, Polynomial diffeomorphisms of $\mathbf{C}^2$ VI: Connectivity of J, Annals of Math., **148** (1998), 1–41.

[BS3]   E. Bedford and J. Smillie, Polynomial diffeomorphisms of $\mathbf{C}^2$ VIII: Quasi-expansion, in press, Amer. J. Math. (2002).

[BS4]   E. Bedford and J. Smillie, Real Polynomial Diffeomorphisms with Maximal Entropy: Tangencies.

[BS5]   E. Bedford and J. Smillie, Real Polynomial Diffeomorphisms with Maximal Entropy: II. Small Jacobian.

[BS6]   E. Bedford and J. Smillie, External rays in polynomial automorphisms of $\mathbf{C}^2$, Contemporary Mathematics, **222** (1999), 41–79.

[BC]   M. Benedicks and L. Carleson, Dynamics of the Hénon map, Annals of Math., **133** (1991), 73–169.

[DF]   J. Diller and C. Favre, Dynamics of bimeromorphic maps of surfaces, Amer. J. Math., **123** (2001), 1135–1169.

[EM]   H. El Hamouly and C. Mira, Lien entre les propriétés d'un endomorphisme de dimension un et celles d'un difféomorphisme de dimension deux, C. R. Acad. Sci. Paris Sér. I Math., **293** No. 10 (1981), 525–528.

[FG1]   J-E Fornæss and E. Gavosto, Existence of homoclinic tangencies for Henon mappings, J. of Geometric Analysis, **2** (1992), 429–444.

[FG2]   J-E Fornæss and E. Gavosto, Tangencies for real and complex Hénon maps: An analytic method, Experimental math., **8** (1999), 253–260.

[F]   S. Friedland, Entropy of algebraic maps, Proceedings of the Conference in Honor of Jean-Pierre Kahane (Orsay, 1993), J. Fourier Anal. Appl. (1995), 215–228.

[FM]   S. Friedland and J. Milnor, Dynamical properties of plane polynomial automorphisms, Ergod. Th. & Dynam. Sys., **9** (1989), 67–99.

[H]   M. Hénon, A two-dimensional mapping with a strange attractor, Commun. Math. Phys., **50** (1976), 69–77.

[HO]   J.H. Hubbard and R. Oberste-Vorth, Hénon mappings in the complex domain II: Projective and inductive limits of polynomials, in "Real and Complex Dynamical Systems (Eds. B.

Branner and P. Hjorth)", Kluwer Academic Publishers, 1995, pp. 89–132.

[HP]   J.H. Hubbard and K. Papadantonakis, Exploring the parameter space of complex Hénon mappings, to appear in Experimental Mathematics.

[MNTU]   S. Morosawa, Y. Nishimura, M. Taniguchi and T. Ueda, "Holomorphic Dynamics", Cambridge U. Press, 2000.

[O]   R. Oliva, On the combinatorics of external rays in the dynamics of the complex Hénon map, PhD Thesis, Cornell University.

[RS]   D. Ruelle and D. Sullivan, Currents, flows and diffeomorphisms, Topology, **14** (1975), 319–327.

[S]   N. Sibony, Dynamique des applications rationnelles de $\mathbf{P}^k$, Panoramas et Synthèses, **8** (1999), 97–185.

Department of Mathematics
Indiana University
Bloomington, IN 47405
USA